Evaluation of the Level of Fit of Radial Fracture Fixation Plates Using Virtual and 3D-printed Models

Sorin Siegler (sieglers@drexel.edu)
Drexel University College of Engineering https://orcid.org/0000-0002-7312-5774
Jordan Stolle
Drexel University College of Engineering
Asif Ilyas
Rothman Orthopaedic Institute at Jefferson: Rothman Orthopaedic Institute
Nicholas Marcouiller
Drexel University College of Engineering
Christopher M. Jones
Rothman Orthopaedic Institute at Jefferson: Rothman Orthopaedic Institute

Research Article

Keywords: Fracture Fixation Plate, Radius, Level of Fit, Virtual models, 3D printed Bone models

Posted Date: May 10th, 2021

DOI: https://doi.org/10.21203/rs.3.rs-445763/v1

Abstract

Radial fractures often require surgical stabilization with fracture fixation plates. Incomplete morphological reconstruction was linked to poor outcome such as limited forearm rotation. Pre-contoured plates are often used, but large inter-subject morphological variations may result in poor fit. Therefore, the goal of this study was to develop a reliable virtual measure of plate-to-bone fit. In addition, the study evaluated the accuracy with which 3D printed bones reproduce the morphology of the physical radius. Virtual models and 3D-printed models of six cadaver radii were produced from bone scans. Level of fit of pre-contoured plates were measured in three ways: directly on pre-contoured physical plates fitted to cadaver bone; pre-contoured physical plates fitted to 3D printed bone; and virtual plate models fitted to virtual bone models. In addition, the study evaluated the accuracy with which 3D printed bone reproduces the physical bone morphology. The results indicate excellent agreement between the physical and virtual level of fit measures as well as excellent geometrical accuracy of the 3D-printed bones. These provide the necessary foundation for guiding the development of better fitted pre-contoured fracture fixation plates as well as for developing pre-surgically patient specific pre-contoured plates.

Authors Biography

Sorin Siegler is a professor Mechanical Engineering and Biomechanics at Drexel University. His research is in Orthopedic Biomechanics and he published extensively in Biomechanics and Orthopedic professional journals.

Jordan Stolle is a graduate student at Drexel University pursuing his PhD degree in Biomechanics under the supervision of Sorin Siegler. He has BSc and MSc degrees in Mechanical Engineering.

Asif Ilyas is an orthopedic surgeon with specialization in hand surgery at Thomas Jefferson University. He is a professor and the program director of Hand and Upper Extremity Fellowship and the president of the Pennsylvania Orthopedic Society.

Nicholas Marcouiller is a graduate student at Drexel University pursuing his PhD degree in Biomechanics under the supervision of Professor James Tangora. He has his BSc and MSc degrees in Mechanical Engineering.

Christopher James is an orthopedic surgeon with specialization in hand and upper extremity surgery at the Rothman Institute. He is an associate professor at Thomas Jefferson University. He has BSc and MSc degrees in Mechanical Engineering.

Introduction

Fractures of the radius bone in adults are unstable injuries that typically require surgical stabilization with bone plates and screws. As with other fracture surgery, restoring normal anatomic alignment is a primary goal. This is especially true of forearm diaphyseal fracture fixation where the bowed radius rotates nearly

180° about the ulna [1, 2]. Accordingly, incomplete reconstitution of the radial bow during fracture surgery in both location and magnitude has been linked to reduced forearm rotation and suboptimal functional outcomes as well as altered kinematics [3–10]

A radius bone plate often requires contouring in the sagittal, coronal, and axial planes, to match the three-dimensional radial bow [3, 4, 7, 11, 12]. The radius of curvature is most pronounced on the volar and dorsal aspects of the bone, corresponding with the two most common surgical approaches to a radial shaft fracture. The standard plate used for adult diaphyseal forearm fractures is a limited-contact dynamic compression plate [13–16]. Contouring this relatively rigid plate in 3 planes can be complex and time consuming [17, 18].

To simplify the plating procedure, pre-contoured plates for volar and dorsal surfaces of the radial shaft have been recently introduced [17, 18]. Pre-contoured plates eliminate or reduce plate-bending time in the operating room. Also, these plates may obviate the need for a provisional fracture reduction. If the pre-contoured plate matched the contour of the intact bone, the plate could be used as a template to which the bone can be reduced, instead of a first needing a provisional reduction which would then guide plate contouring.

There is substantial inter-subject variability in the curvature of the radius bone as demonstrated by a recent morphological study conducted on 422 cadaver radii [7] and because of this large variability, pre-contoured plates may not fit as well as surgeon contoured plates. Furthermore, in highly comminuted fractures, the original shape of the fractured bone is difficult to assess and it relies on the surgeon's experience to restore the original contour.

There are two novel methods for addressing the requirement for time efficient, anatomical fit of radial fracture fixation plates. Both rely on the high level of left-to-right symmetry in the morphology of the radius [19, 20]. The first method is based on producing a 3D printed model of the mirrored, intact, contra-lateral radius and providing it to the surgeon so that, prior to the surgery, the plate can be pre-contoured for optimal fit. This method relies on the ability to produce accurate, image-based, 3D printed models of the physical bone. A primary goal of this study is to test the level of accuracy with which such a 3D printed model can be produced.

The second method is to produce a patient-specific, optimally fitted, fracture fixation plate [21] based on the mirrored contra-lateral intact bone. However, this custom manufacturing approach would undoubtedly be costly and time-consuming, and potentially only a viable option for complex revision surgeries. Therefore, it is prudent to evaluate to what extent an off-the-shelf, pre-contoured fracture fixation plates fits the radius anatomy of a large patient population. To conduct such an evaluation, on a large number of physical cadaver bones, is costly and time prohibitive. Therefore, the second goal of this study was to establish a method of virtually evaluating the fit of fracture fixation plates by applying virtual three-dimensional models of such plates to virtual radius bone models produced from medical imaging scans.

Materials And Methods

Pre-contoured dorsal and volar radial shaft fracture fixation plates were obtained from the manufacturer (Acumed™). In each plate, an array of 27, 1.5 mm holes were drilled through the plate across its surface (Fig. 1). These holes allowed physical measurements of the gap distribution (level of fit) between the surface of the plate and the surface of the bone. Three-dimensional CAD models of the plates were also obtained from the manufacturer, and an identical array of 1.5 mm holes was produced in each virtual CAD model (Fig. 1). These virtual models, together with virtual models of the bones, provided virtual measures of plate-to-bone fit and allowed a direct comparison to the physical measurements.

Six fresh frozen cadaver arms were thawed to room temperature and the radii were extracted and cleaned of soft tissue. Each radius was visually inspected to confirm that no prior fracture or deformities were present. They were coated with non-reflective paint and the midpoint between the proximal and distal ends of the bones were marked (Fig. 2). In addition, three small 1.5 mm diameter holes were drilled at each end of the bone and 1.5 mm metal pins were press-fitted into each hole protruding approximately 1.5 mm from the surface of the bone (Fig. 2). These pins were used as fiduciary markers to reproduce the physical alignment of the plate on the bone in the 3D printed bones and in the virtual models. The bones were scanned using a laser scanner (Artec Space Spider Scanner™; accuracy 0.05 mm; resolution 0.1 mm) and the scanned data were processed (Geomagic™) to obtain 3D models of the bones (Fig. 2). Three dimensional prints of each of the bones were produced (Connex Object500 by Stratasys, material VeroPureWhite RDG837, Resolution 30 microns, Accuracy 200 microns) and each of the 3D prints were scanned to obtain virtual models of the 3D printed bones.

The dorsal and volar plates were fixed to the dorsal and volar sides of each bone with the plate center aligned with the previously marked mid-distance between the distal and proximal ends of the bone (Fig. 3). While maintaining this central alignment, the plate could still be slightly adjusted circumferentially on the bone to improve fit as judged and accomplished by a fellowship-trained hand surgeon. Once this alignment was established, the plates were secured with one screw on each end. Care was taken not to overtighten the screws so as not to deform the plate (Fig. 3, PD and PV). The distances between the central and most distal holes, on each side of the plate, and the corresponding three fiduciary markers (d_1 to d_6 in Fig. 3) was measured with a caliper (Mitutoyo™, 0.01 mm accuracy). These distances were used to reproduce the position of the plates on each of the three-dimensional printed bones, as well as to reproduce the position of the virtual plates on the virtual bones (Fig. 3, VD and VV).

Using a digital depth-gage micrometer (Mitutoyo™, 0.01 mm accuracy) with a spindle diameter of 1.5 mm, the distance between the top surface of the plate (the one away from the bone) and the surface of the bone was measured at each of the 27, 1.5-mm drilled holes (Fig. 4, A). Each distance measurement was repeated three times and the average of the three measurements was used in the subsequent calculations. The gap distance between the bone and the plate at each of the 27 locations was then calculated based on the micrometer measures and the known plate dimensions. Using the central distal holes-to-fiduciary markers measurements (d_1 to d_6 in Fig. 3), the plate positions on the bones were

reproduced on each of the 3D printed bones. Then, after fixation of the plate to the 3D printed bone, the physical plate-to-bone gap measurement at each of the 27 holes was repeated. Using the distances to the fiduciary markers (d_1 to d_6 in Fig. 3), the position of the plates on the virtual model of each bone was reproduced (Fig. 3, VD and VV). Then the virtual plate-to-bone distance at each of the 27 holes was measured by aligning a 1.5 mm diameter cylinder into each hole and measuring the distance from the underside of the plate at the specific hole to the point where the cylinder contacts the surface of the bone (Fig. 4, B). This allowed direct comparison of the plate-to-bone distance distribution between the physical and virtual conditions.

In each virtual plate (dorsal and volar), the limited bone contact region (the visible slightly elevated region in the physical models and the marked regions on each virtual plate in Fig. 1) was identified and marked (Geomagic™). This slightly elevated region on the plate was designed to be the only surface to contact the bone. For each of these regions, distance maps [22] describing the distance distribution between the bone limited contact region of the plate and the corresponding surface of the bone were obtained for both the dorsal side and the volar side of the bone (Fig. 5).

Using an optimal alignment algorithm based on least square error criterion in Geomagic™, for each specimen, the virtual model of the physical bone and the virtual model of the 3D printed bone were optimally aligned to each other. Distance maps describing the distance distribution between the two were generate (Fig. 6).

Data Processing

The 3D geometry of the optimally aligned virtual model of each physical bone and the corresponding virtual model of the 3D printed bone were compared to each other. The comparison was based on the distance distribution over the entire surfaces of the models described as distance maps (Fig. 6). From these, for each specimen, the mean distance and the standard deviation of the distance distribution were calculated. In addition, the volume of the virtual model of the physical bone and the 3D printed bone were calculated, and a paired t-test was performed to determine if there were significant differences in volume between the physical bone and the corresponding 3D printed bone.

The level of fit of the fracture fixation plate to the radius was quantified as the average and standard deviation of the plate-to-bone distance as measured across the 27 -hole array in the plates. For the virtual case, it was also quantified as the average distance and standard deviation across the distance between the bone limited contact region of the plate and the corresponding surface of the bone. Repeated Measure Analysis of Variance (ANOVA) was performed on the average and standard deviation distance between the plate and the bone for three different conditions. Physical bones, virtual bones, and 3D printed bones. The statistical significance level was set at $p < 0.05$. The analysis was performed separately for the volar side and for the dorsal side of the radius. A separate paired t-test was conducted for the virtual plate assessment to compare the level of fit as obtained from the 27-hole array

measurements to that obtained from the distance map. This analysis provided a measure of how well the 27-hole array measurements approximated the full bone limited contact region.

Results

An example showing the distance map between the virtual model obtained from the physical bone and a virtual model obtained from the corresponding 3D printed bone shows a close match with an error of less than 0.5 mm (Figure 6). The distance error distribution obtained from all specimens (Table 1) shows a very small average error of 0.129 mm with a standard deviation of 0.128 mm. Likewise, there was a close match, with no statistical difference (P = 0.239) in volume between the two models with an average error of only 6.8% (Table 1).

The level of fit of the pre-contoured fracture fixation plates to the radius on both the dorsal side (Table 2) and the volar side (Table 3) of the bone under three different conditions were compared. The comparison, based on repeated measure ANOVA, conducted on the average gaps obtained from the 27-hole arrays, showed no statistically significant difference between the three conditions. However, a statistically significant difference (p = 0.004) was observed between the level of fit of the pre-contoured plates on the dorsal side as compared to the level of fit on the volar side, for all three conditions (Table 2 and Table 3).

A paired t-test was conducted for the virtual plate assessment to compare the level of fit as obtained from the 27-hole array measurements to that obtained from the distance map analysis. This t-test provided a measure of how well the 27-hole array measurements approximated the full bone limited contact region. The results show no significant difference between the two. However, the average distance based on the distance maps were smaller than those from the 27-hole array for both dorsal side (Table 2) and the volar side (Table 3).

Discussion

Open reduction and internal fixation with limited-contact compression plates are the most common technique for treating radial and ulnar shaft fractures. Aside from stabilization, restoring normal anatomic alignment is critical. Incomplete reconstitution of the pre-injury morphology of the fractured bones, such as radial torsion and bow of the radius, has been linked to reduced forearm motion and suboptimal kinematic functional outcomes.

While fixation of an ulnar diaphyseal fracture can usually be performed with a straight plate, fixation of the radius is more complex and often requires a plate contoured in the sagittal, coronal, and potentially axial planes, to match the 3-dimensional radial bow. Hence, our focus in this study was on fixation of radial fractures.

In this study a virtual, in-silico technique, for evaluating the level of fit of radial fracture fixation plates was developed. This unique technique was based on quantifying the gap between the plate and the bone surface over both a discrete array as well as over the covered bone surface using distance maps [22]. The

technique was successfully validated by comparing the virtual level of fit to the physical one based on direct measurements performed on the physical bones. The results suggest that the level of fit of pre-contoured fracture fixation plates is significantly better on the dorsal side than on the volar side of the radius. This suggests that the pre-contoured volar fracture fixation plates may benefit from further geometrical design refinement to improve the level of fit.

The evaluation technique established and validated in this study based on virtual and physical distance maps can be adopted to a wide range of orthopedic applications in which artificial surfaces are fixed to physical bones or even replace them. Recent advances in fast and accurate three-dimensional medical imaging modalities, combined with recent developments in additive manufacturing makes personalized surgery an emerging viable reality. For example, personalized fracture fixation plates are already used clinically in reconstructive surgery for the treatment of complex malunions. 3D printed personalized templates for surgical planning required for clinical applications such as producing osteotomies or producing optimal cuts for implants are another area of increased clinical interest. For these and similar applications, the technique developed and validated in this study may be applied both for improved design and for design validation.

This study demonstrated, using the distance mapping technique, that the 3D printed bone very accurately duplicated the three-dimensional geometry of the physical bone. Therefore, since the bi-lateral symmetry in the geometry of the radius has been demonstrated in the past [7, 19, 20], the contra-lateral bone can serve as a reliable replacement for the pre-injury geometry of the fractured bone. This method has been used in recent years for design of personalized total bone replacement such as replacement of the talus [23] and for design of personalized fracture fixation plates. Accurate production of artificial bones that faithfully reproduce the 3D morphology of the physical bone can also be used as a viable less costly alternative to personalized plate production by 3D printing the intact mirror-imaged contralateral bone and then bending and fitting a standard plate to serve as a reliable pre-fit plate to be used for fracture reduction and fracture fixation. Furthermore, the ability to reproduce accurate replica of physical bones is important for future biomechanical research, where it is anticipated that 3D printed bones could replace cadaver bones. This offers significant benefits such as replication of bones in destructive testing in repeated-measure experimental designs. It also minimizes or eliminates the need for transport, storage, and disposal facilities required of cadaver physical specimens. They also offer the ability to conduct reliable comparison of various plate deigns since the same exact bone can be used in multiple tests.

The study had a few limitations. One was the small sample size. This was partially compensated by the repeated-measure analysis made possible since each specimen served as its own control. In addition, it must be recognized that some of the methodology in this study requires highly accurate medical imaging modalities such as high-resolution CT and high accuracy 3D printers to produce accurate virtual or 3D printed models. Such facilities may not be readily available, although their number is on the increase as personalized surgery becomes an emerging trend in orthopedic surgery.

Conclusions

From the results of this study it was concluded that a virtual method for assessing the level of fit of fracture fixation plates to the radial bone reliably reproduce the physical measurement. As such, it can be used as an effective evaluation tool to guide the design of improved pre-contoured fracture fixation plate for the radius. It can also be used to guide the production of patient specific plates in the future. In addition, the study concluded that 3D printed models of the radius bone accurately reproduce the bone morphology. Therefore, such 3D printed models can be used by the surgeon to optimally contour the bone to the patient's 3D morphology prior to surgery, therefore potentially reducing surgical time and improving surgical outcome. Such 3D printed surrogates can also be used as inexpensive and convenient substitutes to physical cadaver bones in a variety of biomechanical studies.

Declarations

- The authors have no relevant financial or non-financial interests to disclose.
- The authors have no conflicts of interest to declare that are relevant to the content of this article.
- All authors certify that they have no affiliations with or involvement in any organization or entity with any financial interest or non-financial interest in the subject matter or materials discussed in this manuscript.
- The authors have no financial or proprietary interests in any material discussed in this article.

All authors contributed to the study conception and design. Material preparation, data collection and analysis were performed by Sorin Siegler, Jordan Stolle, Asif Ilyas, Nicholas Marcouiller, Christopher M. Jones. The first draft of the manuscript was written by Sorin Siegler and all authors commented on previous versions of the manuscript. All authors read and approved the final manuscript.

References

1. King, G.J., et al., *Kinematics of the distal radioulnar joint.* J Hand Surg Am, 1986. **11**(6): p. 798-804.
2. Weinberg, A.M., et al., *A new kinematic model of pro- and supination of the human forearm.* J Biomech, 2000. **33**(4): p. 487-91.
3. Dumont, C.E., R. Thalmann, and J.C. Macy, *The effect of rotational malunion of the radius and the ulna on supination and pronation.* J Bone Joint Surg Br, 2002. **84**(7): p. 1070-4.
4. Firl, M. and L. Wunsch, *Measurement of bowing of the radius.* J Bone Joint Surg Br, 2004. **86**(7): p. 1047-9.
5. Fraser, G.S., et al., *The effect of multiplanar distal radius fractures on forearm rotation: in vitro biomechanical study.* J Hand Surg Am, 2009. **34**(5): p. 838-48.
6. Rupasinghe, S.L. and P.C. Poon, *Radius morphology and its effects on rotation with contoured and noncontoured plating of the proximal radius.* J Shoulder Elbow Surg, 2012. **21**(5): p. 568-73.
7. Weber, M.B., et al., *A cadaveric study of radial and ulnar bowing in the sagittal and coronal planes.* J Shoulder Elbow Surg, 2020. **29**(5): p. 1010-1018.

8. Crisco, J.J., et al., *Effects of distal radius malunion on distal radioulnar joint mechanics--an in vivo study.* J Orthop Res, 2007. **25**(4): p. 547-55.
9. Moore, D.C., et al., *Three-dimensional in vivo kinematics of the distal radioulnar joint in malunited distal radius fractures.* J Hand Surg Am, 2002. **27**(2): p. 233-42.
10. Bronstein, A.J., T.E. Trumble, and A.F. Tencer, *The effects of distal radius fracture malalignment on forearm rotation: a cadaveric study.* J Hand Surg Am, 1997. **22**(2): p. 258-62.
11. Holweg, P., et al., *Comparison of volar and dorsal plate osteosynthesis for radial shaft fractures: an anatomical pilot study.* Injury, 2017. **48 Suppl 5**: p. S38-S40.
12. Yorukoglu, A.C., et al., *The effects of radial bowing and complications in intramedullary nail fixation of adult forearm fractures.* Eklem Hastalik Cerrahisi, 2017. **28**(1): p. 30-4.
13. Anderson, L.D., et al., *Compression-plate fixation in acute diaphyseal fractures of the radius and ulna.* J Bone Joint Surg Am, 1975. **57**(3): p. 287-97.
14. Leung, F. and S.P. Chow, *A prospective, randomized trial comparing the limited contact dynamic compression plate with the point contact fixator for forearm fractures.* J Bone Joint Surg Am, 2003. **85**(12): p. 2343-8.
15. Leung, F. and S.P. Chow, *Locking compression plate in the treatment of forearm fractures: a prospective study.* J Orthop Surg (Hong Kong), 2006. **14**(3): p. 291-4.
16. Chapman, M.W., J.E. Gordon, and A.G. Zissimos, *Compression-plate fixation of acute fractures of the diaphyses of the radius and ulna.* J Bone Joint Surg Am, 1989. **71**(2): p. 159-69.
17. Bishop, J.A., et al., *Contouring Plates in Fracture Surgery: Indications and Pitfalls.* Journal of the American Academy of Orthopaedic Surgeons, 2020. **28**(14): p. 585-595.
18. Downing, N.D. and A. Karantana, *A revolution in the management of fractures of the distal radius?* J Bone Joint Surg Br, 2008. **90**(10): p. 1271-5.
19. Gray, R.J., et al., *Image-Based Comparison Between the Bilateral Symmetry of the Distal Radii Through Established Measures.* J Hand Surg Am, 2019. **44**(11): p. 966-972.
20. Vroemen, J.C., et al., *Three-dimensional assessment of bilateral symmetry of the radius and ulna for planning corrective surgeries.* J Hand Surg Am, 2012. **37**(5): p. 982-8.
21. Dobbe, J.G., et al., *Patient-specific distal radius locking plate for fixation and accurate 3D positioning in corrective osteotomy.* Strategies Trauma Limb Reconstr, 2014. **9**(3): p. 179-83.
22. Siegler, S., et al., *Analysis of surface-to-surface distance mapping during three-dimensional motion at the ankle and subtalar joints.* J Biomech, 2018. **76**: p. 204-211.
23. Akoh, C.C., J. Chen, and S.B. Adams, *Total Ankle Total Talus Replacement Using a 3D Printed Talus Component: A Case Report.* J Foot Ankle Surg, 2020.

Tables

Table 1 – Comparison of the 3D geometry of the physical radial bone to the 3D geometry of the 3D printed radial bone. All measurements are in Millimeters.

				Error Distance Distribution between model of physical bone and model of 3D printed bone	
Specimen #	**Volume[mm3] physical Bone**	**Volume [mm3] virtual Bone**	**% error volume**	**Average [mm]**	**STDV [mm]**
1	37704	44373	17.69	.23	.49
2	25717	27703	7.72	.20	.24
3	21573	22688	5.17	.25	.40
4	30209	31503	4.28	.10	.28
5	30669	29037	5.32	.51	.55
6	32410	32215	.601	.17	.21
Average	**29714**	**31253**	**6.8**	**.243**	**.362**
STDV	**5074**	**6633**	**5.3**	**.129**	**.128**

Table 2: Comparison of the plate-to-bone level of fit on the dorsal side of the radius based on the 27 distance measurements for three conditions – Physical measurement on physical bone, virtual measurements on virtual bone, and physical measurements on 3D printed bone.

	Physical Measurements (27-hole array) on physical bone		Physical Measurements (27-hole array) on 3D printed bone		Virtual measurements (27-hole array) on virtual bone		Virtual Measurements (Distance Map) on virtual bone	
Specimen	Avg. [mm]	STDV [mm]	Avg. [mm]	STDV [mm]	Avg. [mm]	STDV [mm]	Avg [mm]	STDV [mm]
1	0.78	0.54	2.02	1.49	1.17	0.56	1.08	0.75
2	0.94	0.78	0.76	0.57	2.17	0.9	1.96	1.42
3	1.38	0.8	1.11	0.68	2.54	0.78	1.99	0.78
4	0.76	0.57	0.9	0.72	1.44	0.61	1.09	0.68
5	1.07	0.62	1.42	1.17	1.73	0.72	1.35	0.58
6	1.02	0.62	0.72	0.53	1.13	0.43	0.72	0.46
Average	**0.99**	**0.66**	**1.16**	**0.86**	**1.7**	**0.67**	**1.37**	**0.778**
STDV	**0.23**	**0.1**	**0.5**	**0.353**	**0.52**	**0.154**	**0.47**	**0.306**

Table 3: Comparison of the plate-to-bone level of fit on the volar side of the radius based on the 27 distance measurements for three conditions – Physical measurement on physical bone, virtual measurements on virtual bone, and physical measurements on 3D printed bone.

	Physical Measurements (27-hole array) on physical bone		Physical Measurements (27-hole array) on 3D printed bone		Virtual measurements (27-hole array) on virtual bone		Virtual Measurements (Distance Map) on virtual bone	
Specimen	Avg. [mm]	STDV [mm]	Avg. [mm]	STDV [mm]	Avg. [mm]	STDV [mm]	Avg [mm]	STDV [mm]
1	1.68	0.71	1.73	0.81	1.9	0.77	1.4	0.91
2	1.84	0.69	1.46	0.7	2.2	0.6	1.65	1.87
3	1.81	0.92	1.46	0.4	2.37	0.53	1.63	0.43
4	1.85	0.68	1.65	0.6	1.79	0.5	1.15	0.52
5	2.64	1.32	2.8	1.3	2.91	1.29	2.32	1.39
6	3.08	1.27	3.1	1.39	3.03	0.94	2.56	1.1
Average	**2.15**	**0.93**	**2.03**	**0.87**	**2.37**	**0.77**	**1.785**	**1.037**
STDV	**0.57**	**0.27**	**0.73**	**0.352**	**0.47**	**0.276**	**0.497**	**0.496**

Figures

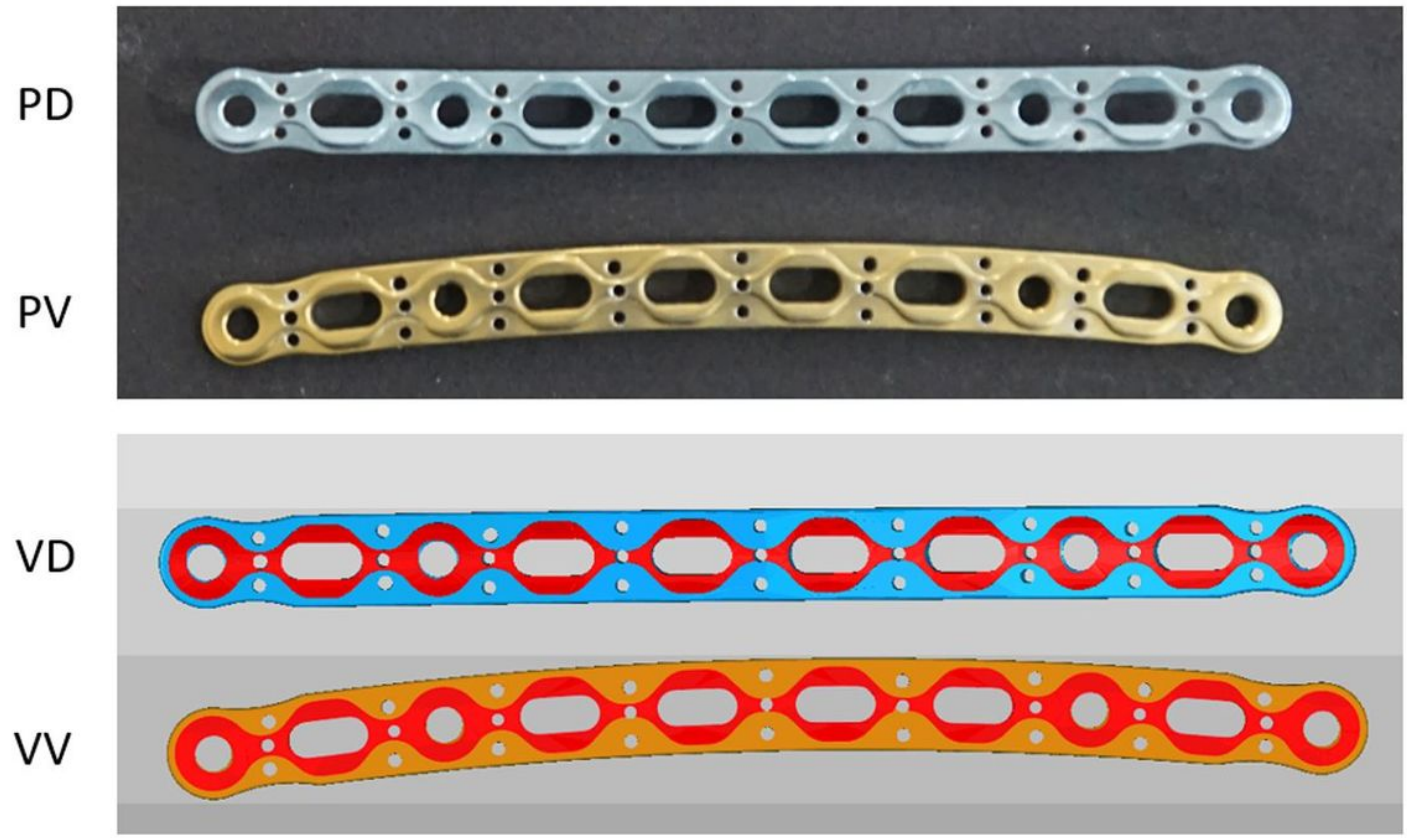

Figure 1

Physical and virtual pre-contoured dorsal and volar radial shaft fixation plates with an array of 27, 1.5 mm in each for plate-to-bone surface gap measurements. PD – Physical Dorsal; PV – Physical Volar, VD – Virtual Dorsal, VV – Virtual Volar. The bone contact region of the plates and visible in the physical plates and marked in the virtual plate images

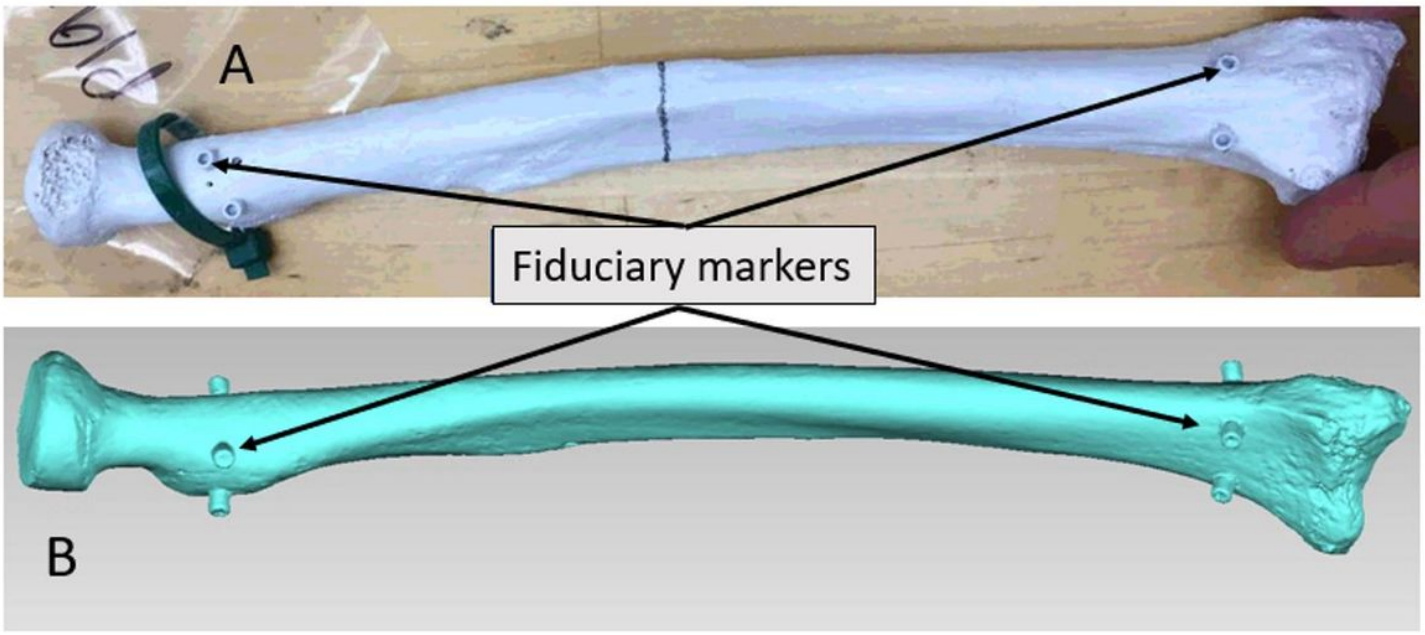

Figure 2

Example of the extracted physical bone (A) and the scanned virtual model (B). The fiduciary markers are visible in both the physical bone and the scanned virtual bone model

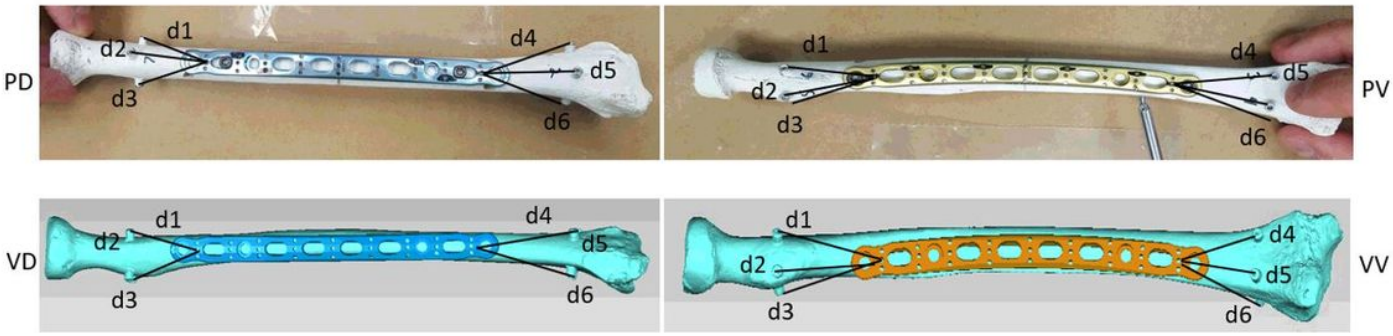

Figure 3

Views of the pre-contoured plates fixed to the dorsal and volar sides of the radius. PD – Physical Dorsal; PV – Physical Volar, VD – Virtual Dorsal, VV – Virtual Volar. The distances between the central and most distal hole and each fiduciary marker are indicated as d1 to d6

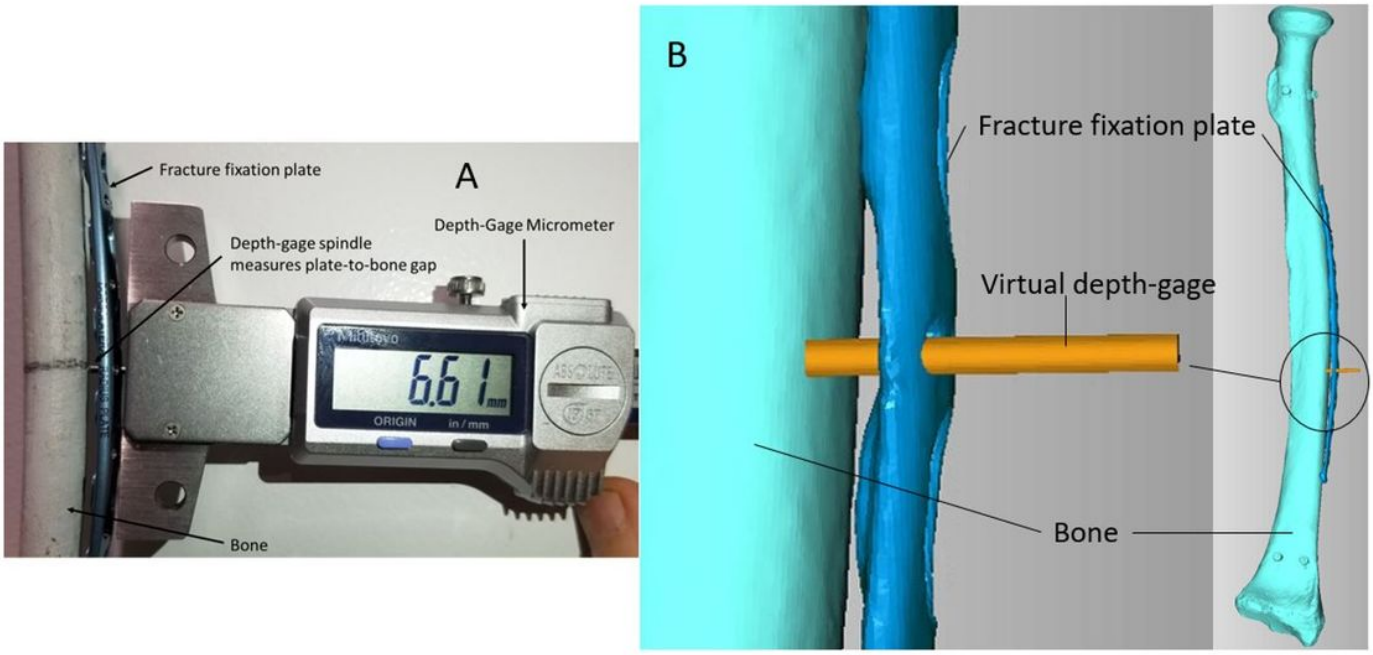

Figure 4

Depth-gage micrometer setup (A) used to measure the gap between the plate and the surface of the bone, and a virtual gage used to simulate these measurements in the 3d virtual environment (B)

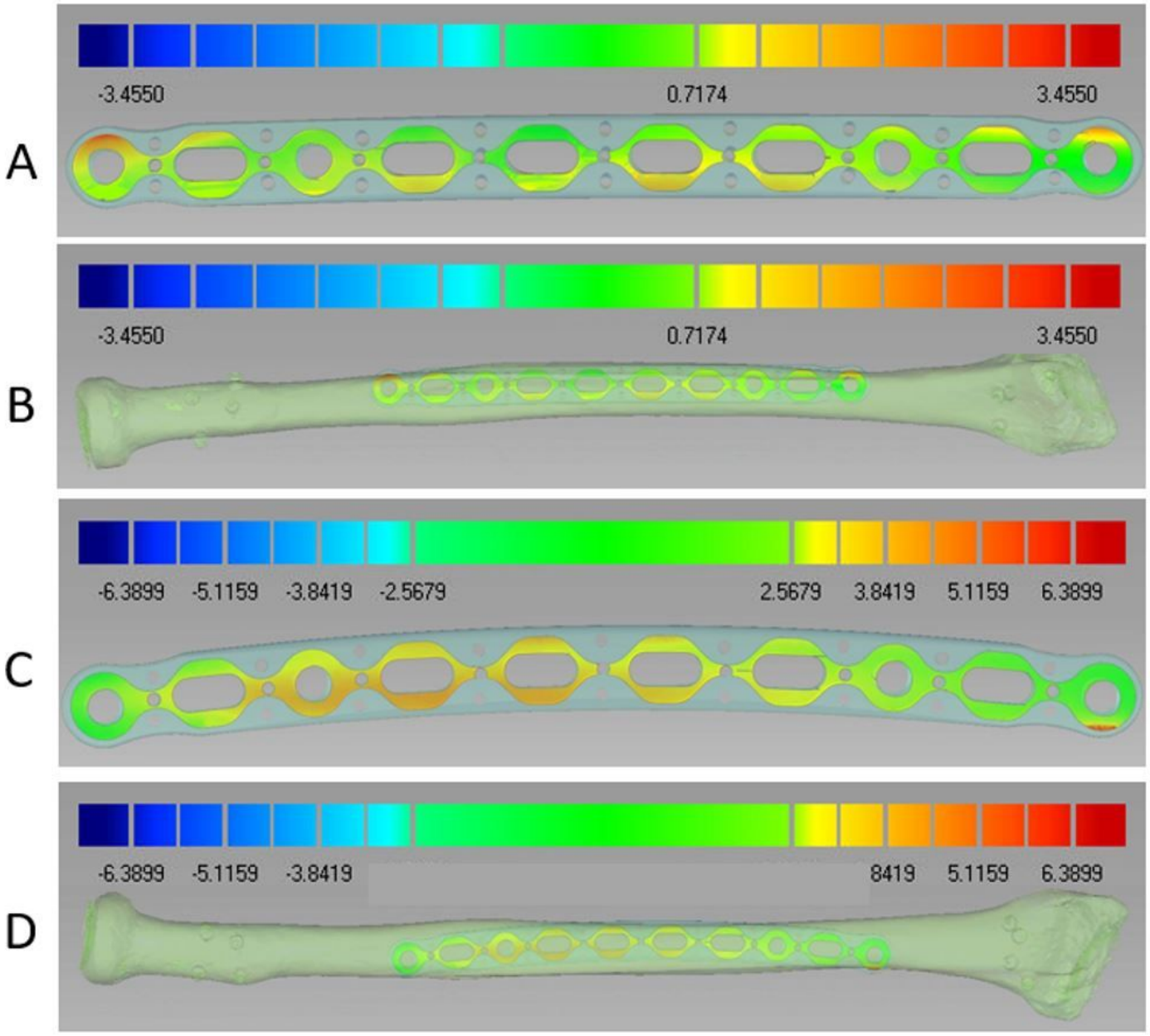

Figure 5

Limited bone contact regions with the corresponding distance maps for the pre-contoured dorsal plate displayed on the plate (A) and on the bone (B). Limited bone contact regions with the corresponding distance maps for the pre-contoured volar plate displayed on the plate (C) and on the bone (D)

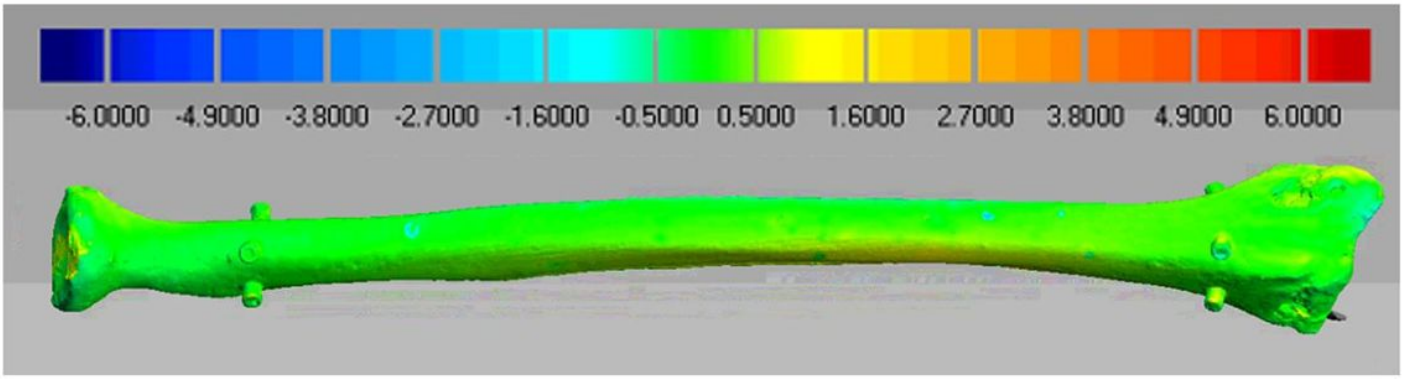

Figure 6

models of the physical and the 3D printed bone optimally aligned to each other and the distance between them in millimeters displayed as color-coded distance maps. Distance color-coded scale is in millimeters